frontiers
in Cellular Neuroscience

Increased 20-HETE Signaling Suppresses Capillary Neurovascular Coupling After Ischemic Stroke in Regions Beyond the Infarct

Zhenzhou Li[1,2†], Heather L. McConnell[3†‡], Teresa L. Stackhouse[3], Martin M. Pike[4],
Wenri Zhang[5] and Anusha Mishra[1,3]*

[1] *Knight Cardiovascular Institute, Oregon Health & Science University, Portland, OR, United States,* [2] *Department of Anesthesiology, General Hospital of Ningxia Medical University, Ningxia, China,* [3] *Department of Neurology, Jungers Center for Neurosciences Research, Oregon Health & Science University, Portland, OR, United States,* [4] *Advanced Imaging Research Center, Oregon Health & Science University, Portland, OR, United States,* [5] *Department of Anesthesiology and Perioperative Medicine, Oregon Health & Science University, Portland, OR, United States*

Neurovascular coupling, the process by which neuronal activity elicits increases in the local blood supply, is impaired in stroke patients in brain regions outside the infarct. Such impairment may contribute to neurological deterioration over time, but its mechanism is unknown. Using the middle cerebral artery occlusion (MCAO) model of stroke, we show that neuronal activity-evoked capillary dilation is reduced by ~75% in the intact cortical tissue outside the infarct border. This decrease in capillary responsiveness was not explained by a decrease in local neuronal activity or a loss of vascular contractility. Inhibiting synthesis of the vasoconstrictive molecule 20-hydroxyeicosatetraenoic acid (20-HETE), either by inhibiting its synthetic enzyme CYP450 ω-hydroxylases or by increasing nitric oxide (NO), which is a natural inhibitor of ω-hydroxylases, rescued activity-evoked capillary dilation. The capillary dilation unmasked by inhibiting 20-HETE was dependent on PGE2 activation of endoperoxide 4 (EP4) receptors, a vasodilatory pathway previously identified in healthy animals. Cortical 20-HETE levels were increased following MCAO, in agreement with data from stroke patients. Inhibition of ω-hydroxylases normalized 20-HETE levels *in vivo* and increased cerebral blood flow in the peri-infarct cortex. These data identify 20-HETE-dependent vasoconstriction as a mechanism underlying capillary neurovascular coupling impairment after stroke. Our results suggest that the brain's energy supply may be significantly reduced after stroke in regions previously believed to be asymptomatic and that ω-hydroxylase inhibition may restore healthy neurovascular coupling post-stroke.

Keywords: neurovascular coupling, stroke, cerebral blood flow, capillaries, microvasculature

INTRODUCTION

Neuronal activity in the central nervous system is coupled to an increase in local blood flow (Attwell et al., 2010; Mishra, 2017). This process, known as neurovascular coupling, ensures that the increased energy demand of active neural tissue is met by a supply of metabolic substrates such as oxygen and glucose. Neurovascular coupling is impaired in many neurodegenerative conditions, including Alzheimer's disease (AD), amyotrophic lateral sclerosis, and multiple sclerosis (Nelson et al., 2016; Iadecola, 2017; Joo et al., 2017; Kotliar et al., 2017). Impaired neurovascular coupling is also reported in patients diagnosed with stroke (Krainik et al., 2005; Lin et al., 2011; Salinet et al., 2015), especially strokes arising from occlusion of the middle cerebral artery (MCA; Salinet et al., 2018). Importantly, neurovascular coupling impairment is observed in stroke patients even when they are considered to be fully recovered, for up to several years following the stroke and in clinically asymptomatic regions outside the infarct lesion (Krainik et al., 2005). This impairment could result in energy deficits in otherwise healthy brain regions and thereby compromise neuronal health over time.

Ischemic injuries, including stroke, transient ischemic attacks, silent infarcts, and watershed microinfarcts, increase the risk of dementia by several fold (Miklossy, 2003; Vermeer et al., 2007; Levine et al., 2015; Yang et al., 2015; van Rooij et al., 2016), and this is not explained purely by common risk factors (Savva et al., 2010). Conversely, patients with dementia often show signs of previous ischemic injuries in their brains (Snowdon et al., 1997; Miklossy, 2003; Vermeer et al., 2007). Furthermore, cerebrovascular dysfunction is one of the earliest detectable changes in patients who develop cognitive dysfunction and dementia (Iturria-Medina et al., 2016; Korte et al., 2020). Ischemia-induced impairment of neurovascular coupling is likely a major contributor to such cerebrovascular dysfunction, yet mechanisms underlying this impairment have not yet been studied.

In the healthy brain, neurovascular coupling at the capillary level occurs *via* an astrocyte-mediated pathway that relies on vasoactive metabolites of arachidonic acid. In response to neuronal activity, astrocytes synthesize arachidonic acid and metabolize it to form prostaglandin E2 (PGE2), which then acts on the endoperoxide 4 (EP4) receptor on contractile pericytes to induce capillary dilation (Mishra et al., 2016). Arachidonic acid can also be metabolized to the vasoconstrictive molecule 20-hydroxyeicosatetraenoic acid (20-HETE). The CYP450 ω-hydroxylase enzymes that synthesize 20-HETE are inhibited in physiologically healthy tissue, however, by activity-dependent production of nitric oxide (NO) (Alonso-Galicia et al., 1997; Hall et al., 2014). Thus, neuronal activity leads to a net dilation of capillaries *via* EP4 receptors.

Existing evidence suggests that increased levels of 20-HETE in the cerebrospinal fluid (Crago et al., 2011) and plasma (Yi et al., 2016; Yi et al., 2017) of stroke patients predict a negative clinical prognosis. Further, an increase in 20-HETE synthesis occurs after experimental stroke in rodent models and contributes to a decrease in global cerebral blood flow (CBF) after stroke (Poloyac et al., 2006) and cortical spreading depression (Fordsmann et al., 2013). Evidence also suggests that neuronal and endothelial NO synthases are downregulated after ischemic vascular injury (Zhao et al., 2018). These findings led us to hypothesize that a decrease in NO disinhibits 20-HETE synthesis and thereby impairs neurovascular coupling after stroke.

Here, we applied transient middle cerebral artery occlusion (MCAO) and assayed neurovascular coupling in acute brain slices prepared 1 day after transient MCAO. We found that neuronal activity-induced capillary dilation is severely diminished in intact cortical tissue beyond the infarct border, a region we term the "peri-infarct," compared to the analogous region in the contralateral hemisphere or naïve brains. We show that impairment of neurovascular coupling is not due to decreased neuronal activity or vascular contractility, but rather due to increased synthesis of the vasoconstrictor 20-HETE. Importantly, we demonstrate that preventing 20-HETE synthesis can restore healthy neurovascular coupling *ex vivo* and elevate CBF *in vivo*, selectively in the peri-infarct cortex of the stroke hemisphere. These data suggest a mechanism for neurovascular coupling impairment after stroke in the intact cortex surrounding the infarct, mediated by 20-HETE synthesis.

MATERIALS AND METHODS

Animals
All experiments were approved by the Oregon Health & Science University Institutional Animal Care and Use Committee.

Middle Cerebral Artery Occlusion
Two-month-old Long-Evans rats (Charles River Laboratories) of either sex were randomly assigned to experimental (MCAO) or naïve groups. All animals were in healthy condition prior to manipulation. Rats were placed under isoflurane anesthesia (5% induction and 1.5% maintenance) in 30% oxygen-enriched air *via* mask. Body temperature was maintained at 37 ± 0.5°C throughout the procedure. MCA occlusion was performed using a previously described method with slight modifications (Longa et al., 1989). Briefly, a laser Doppler flowmeter (Moore Instruments) probe was affixed over the right parietal bone overlying the MCA territory to monitor changes in CBF. A ventral midline incision was made over the neck, the right common carotid artery (CCA) bifurcation was exposed by gentle dissection and tissue retraction, and the external carotid artery (ECA) was permanently ligated distal to the occipital artery using electrocautery, such that a short ECA stump remained attached to the bifurcation. The right CCA and internal carotid arteries (ICA) were temporarily closed with reversible slip knots before an arteriotomy was made in the ECA stump. A silicone-coated 5.0 nylon monofilament (Doccol Corporation) appropriate for the weight of the rat, as suggested by the manufacturer, was inserted into the ICA *via* the arteriotomy and gently advanced to the ICA/MCA bifurcation to occlude CBF to the MCA territory at a location confirmed by a laser Doppler signal drop (**Figure 1A**). After 60 min occlusion, the filament was gently retracted, the ECA permanently ligated, the slip knot on the CCA removed,

and the incision sites sutured closed. Animals were housed separately from one another and monitored for several hours post-op to ensure recovery. If no procedural error occurred intraoperatively (vessel puncture and bleeding), essentially 100% of the animals survived to the 1-day post-MCAO time point and were included in the study.

To ensure adequate representation of both sexes, equal numbers of male and female rats were used in all experiments. The data presented herein are pooled by sex. As our study was not powered to detect sex-based differences, these analyses were not performed.

Brain Slice Preparation

Acute brain slices were prepared as described previously (Mishra et al., 2014) from rats 1 day after MCAO surgery. Briefly, 300-μm-thick coronal cortical slices were prepared on a Vibratome in ice-cold oxygenated (95% O_2 and 5% CO_2) solution containing (in mM) 93 N-methyl-D-glucamine (NMDG) chloride, 2.5 KCl, 30 $NaHCO_3$, 10 $MgCl_2$, 1.2 NaH_2PO_4, 25 glucose, 0.5 $CaCl_2$, 20 HEPES, 5 Na ascorbate, 3 Na pyruvate, 2 thiourea, and 1 kynurenic acid. The slices were incubated at 34°C in the same solution for 15–20 min, then transferred to a similar solution with the NMDG chloride, $MgCl_2$, and $CaCl_2$ replaced by (mM) 93 NaCl, 1 $MgCl_2$, and 2 $CaCl_2$, and incubated at room temperature (21–23°C) for at least 20 min or until used in experiments (maximum of 5 h).

Identification and Imaging of Capillaries

Slices were perfused with bicarbonate-buffered artificial cerebrospinal fluid (aCSF) containing (in mM) 124 NaCl, 2.5 KCl, 26 $NaHCO_3$, 1 $MgCl_2$, 2 $CaCl_2$, 1 NaH_2PO_4, 10 glucose, 1 Na ascorbate, warmed to 32–34°C and bubbled with 20% O_2, 5% CO_2, and 75% N_2 to mimic physiologic O_2 conditions and avoid O_2 or metabolism-dependent modulation of vascular responses (Gordon et al., 2008; Mishra et al., 2011; Hall et al., 2014). Imaging was performed using differential interference contrast microscopy with a 40× water immersion objective, a CMOS USB 3.0 camera (Thorlabs), and Micro-Manager acquisition software. Capillaries were imaged at 15–50 μm depth in layers III–VI of slices containing the sensorimotor cortices, in the peri-infarct region (stroke hemisphere) or the analogous region (contralateral and naïve slices) (**Figure 1B**). The peri-infarct region was defined as all dorsomedial cortical regions >0.5 mm away from the infarct border, which is identified as the area comprising dead and swollen cells. Capillaries were defined, as previously described, as vessels with <8 μm luminal diameter and lacking abluminal contiguous smooth muscle cells, often instead containing pericytes identified by their bump-on-a-log morphology at ∼30 μm intervals (Mishra et al., 2014). Images were acquired every 5 s, with 10 ms exposure, at a resolution of 132 nm/pixel. As vessels in acute brain slices lack perfusion and therefore tone, U46619 (200 nM) was applied in the bath for at least 5 min to preconstrict capillaries in all experiments assaying neurovascular coupling. Pre-constriction to U46619 ensured that the vessel was healthy and responsive, therefore lack of constriction to U46619 was an exclusion criterion (Mishra et al., 2016). Vessel internal diameters were measured

by manually placing a measurement line perpendicular to the vessel on the image at locations where constriction to U46619 occurred (presumed regions of active pericyte control) using MetaMorph software. Change in diameter was quantified as a 30 s average centered around the largest response seen after stimulation, normalized to baseline diameter. If changes in focus confounded accurate measurements, experiments were excluded from further analysis. Because of the obviousness of the MCAO's effects on both animal behavior (circling in cage) and tissue health within the infarct in acute slices, experiments could not be performed blind. The need to keep track of the ipsilesional and contralesional slices in the MCAO group further precluded blinding during experiments. Thus, experiments were interleaved between the stroke hemisphere and the contralateral slices from each animal to minimize confounds due to day-to-day and time-from-slicing variability. Experiments in naïve slices were performed on alternate days. To minimize bias, all experiments were conducted by one experimenter and the resulting files were analyzed by an independent investigator blinded to the conditions.

Stimulation Protocol for Brain Slices

Electrical stimulation was applied using an aCSF-filled glass electrode with a wide opening placed in layer I/II of the slice, approximately 300–500 μm from the imaged vessel. Two separate stimulation paradigms were tested (**Supplementary Figures 1C,D**): a 1 s, 100 Hz (high-frequency), and a 3 s, 20 Hz (low-frequency) stimulation with 0.2 ms pulse duration and 200 mA intensity using a constant current stimulator (Digitimer). Both paradigms evoked capillary dilations with the same pharmacology (blocked by NF449) as previously described (Mishra et al., 2016). The low-frequency stimulation was chosen as the physiologically relevant minimal stimulation to evoke neuronal activity in all experiments (**Figures 1–4**). To confirm activation of the neurons, extracellular field recordings were performed near the capillary of interest using a 3–5 MΩ glass electrode filled with aCSF, and only experiments where a field excitatory post-synaptic currents (fEPSC) was detected were used for analysis. The amplitude and slope of the first fEPSC were quantified to compare neuronal activation.

Pharmacology in Brain Slices

For all slice experiments, vessels were pre-constricted with U46619, which acts on thromboxane A_2 receptors and constricts capillaries without altering neuronal activity (Mishra et al., 2016). U46619 was applied for at least 5 min before any further manipulations (application of drugs or electrical stimulation). Capillaries that did not constrict to U46619 were disqualified from analysis to exclude vessels in which contractility may be compromised. The drug of interest was then bath applied for at least 5 min before stimulation-evoked capillary responses were evaluated. Each drug was used at a concentration range 2- to 10-fold higher than its EC_{50}/IC_{50} to ensure its effects without introducing non-specificity.

Preparation of Pharmacological Agents

All drugs were obtained from Millipore Sigma or Cayman Chemicals. Stock solutions of most drugs were prepared in dimethyl sulfoxide (DMSO) at the following concentrations: U46619 10 mM, L-161,982 50 mM, NF449 5 mM, and N-Hydroxy-N′-(4-butyl-2-methylphenyl) formamidine (HET0016) 10 mM. Endothelin-1 was dissolved at 400 μM in ddH$_2$O. Stock solutions of each drug were diluted in aCSF to the final concentration on the day of use (as defined in main text). The final concentration of DMSO was maintained at less than 0.002% in all solutions. Diethylenetriamine NONOate (DETA-NONOate) was prepared freshly each day by dissolving 3.2 mg DETA-NONOate powder in 200 mL aCSF.

Arterial Spin-Labeling Magnetic Resonance Imaging – Data Acquisition

All magnetic resonance (MR) imaging was performed on a Bruker BioSpin 11.75T (Bruker Scientific Instruments, Billerica, MA, United States) small animal MR system with a horizontal bore, 9-cm inner diameter (ID) gradient set (750 mT/m), with a 72 mm ID and 60 mm (length) radiofrequency resonator and an actively decoupled 20 mm Bruker surface coil for transmit/receive. Rats were anesthetized with mask isoflurane (∼1.5%) in 100% oxygen and subjected to lateral tail vein canulation with a 27-gauge Terumo Surflo catheter (Thermo Fisher Scientific). A custom platform/head holder was used to dorsoventrally position the rats and immobilize the head. Body temperature was maintained at 37°C using a biofeedback warm air temperature control system (Small Animal Instruments, Inc.). Respiration rate was monitored using the MR-compatible Monitoring & Gating System (Small Animal Instruments, Inc.) and maintained between 75 and 110 breaths/min by slight tuning of isoflurane level. A coronal T$_2$-weighted 35-slice image set was obtained (spin echo RARE, 256×256 matrix, 138×138 μm in-plane resolution, field of view (FOV) = 3.5×3.5 cm, 0.5 mm slice thickness, TR = 4065 ms, TE$_{effective}$ = 23.6 ms, RARE factor 8, 2 averages). CBF was measured using ASL with flow-sensitive alternating inversion-recovery (FAIR) rapid acquisition with relaxation enhancement pulse sequence (FAIR-RARE), with echo time/repetition time (TE/TR) = 45.2 ms/10,000 ms, FOV = 3.5×3.5 cm, slice thickness = 2 mm, number of slices = 1, matrix = 128×128, RARE factor = 72, and 23 inversion times ranging from 40 to 4400 ms. This sequence labels the inflowing blood by global inversion of the equilibrium magnetization (Kim, 1995) with a total acquisition time of 15 min. In rats exposed to MCAO, the T$_2$-weighted images were used as a localizer to accurately place the ASL slice at the coronal position where maximal infarct volume was observed. For control (naïve) rats, coronal slices known to contain brain regions supplied by the MCA that were comparable in anatomy to those used in MCAO rats were chosen. Following first image capture, volume equivalent doses of either HET0016 (1 mg/kg) or vehicle (DMSO, approximately 1.8% in saline) were then slowly infused over 1 min *via* tail vein catheter. ASL imaging was repeated 30 min after injection. As the infarct in the MCAO group was obvious under T$_2$-weighted images, blinding during ASL-magnetic resonance imaging (MRI) was not possible.

Arterial Spin-Labeling Magnetic Resonance Imaging – Image Analysis

Jim 7.0 image analysis software (Xinapse Systems, United Kingdom) was used for image processing. CBF maps (units: mL/100 g/min) were generated using the Bruker ASL perfusion processing macro, which uses the equation:

$$rCBF = \lambda \cdot \frac{T_1 nonsel}{T_1 blood} \cdot \left(\frac{1}{T_1 sel} - \frac{1}{T_1 nonsel} \right)$$

where λ, the blood-brain partition coefficient (0.9); T$_{1blood}$, the T$_1$ of blood (2800 ms); and T$_{1sel}$ and T$_{1nonsel}$ are the measured T$_1$ values under selective and nonselective inversion conditions, respectively. CBF maps were exported into Jim imaging software for further processing. The ROI (region of interest) toolkit was used to manually outline the entire brain on a paired T$_2$-weighted image slice, which was subsequently divided into left and right hemispheres. Next, the ipsilateral peri-infarct cortex and contralateral analogous cortex ROIs were determined based on the T$_2$-weighted image for each animal taking care to avoid the infarct lesion and the underlying white matter (corpus callosum). The identical FOV and geometry of the T$_2$ and ASL volumes enabled the ROIs to be readily overlaid onto the corresponding perfusion map for quantification. To remove flow contributions from large vessels and better quantify capillary flow, voxels with intensities $\pm$ 2 SD of the mean were excluded. The average of all remaining voxel intensities was then used to calculate corrected flow values within an ROI. To quantify the change in CBF induced by the treatment (vehicle or HET0016), flow values for each ROI after the treatment injection were normalized to pre-treatment values.

Preparation of Samples for 20-Hydroxyeicosatetraenoic Acid and Prostaglandin E2 Measurement

Both 20-HETE and PGE2 are lipid signaling molecules that are synthesized on-demand and can easily pass the membrane to signal to other cells; thus, it is most appropriate to measure whole tissue lysate concentrations. Brains from rats treated with vehicle or HET0016 during the ASL experiment were dissected within 10 min after MRI and 500-μm thick live brain slices were cut using a Vibratome (Leica) spanning the sensorimotor cortex within the MCA territory, as determined visually based on comparison with triphenyl tetrazolium chloride (TTC) stains on other MCAO brains (to define stroke region), the T$_2$ images from the same animal, and the Rat Brain Atlas (Paxinos and Watson). Immediately after cutting, the stroke peri-infarct and analogous cortical regions (from control slices) were carefully microdissected from each slice, excess aCSF was gently wicked away from the tissue with a Kimwipe^{TM}, and the tissue was transferred to a vial containing 1 mL of 0.1% formic acid in water. This was performed in duplicate for each vial, such that each sample contained microdissected cortical regions from two adjacent coronal slices. Two vials were

prepared from each hemisphere of each animal and immediately placed in a $-80°C$ freezer to preserve tissue contents. The frozen vials were blinded and transferred to the Bioanalytical Shared Resource/Pharmacokinetics Core at Oregon Health & Science University.

At the time of measurement, vials were thawed and the tissue homogenized using a BeadBug microtube homogenizer. A 0.9 mL aliquot of the tissue homogenate was placed into a 13×100 mm glass screw-top extraction tube with a Teflon^{TM}-lined cap. The remaining 0.1 mL of the homogenate was used for protein quantification for normalization of the data. Deuterated internal standards were added (1 ng of PGE2-d_9 and 2 ng 20-HETE-d_6) to the homogenate and the tubes were extracted in sequence with 3 mL of ethyl acetate with 0.02 mg/mL triphenylphosphine, followed by 3 mL of a 1:1 mixture of ethyl acetate:hexane, and finally with 2 mL of hexane. The combined supernatants were spiked with 20 μL of a trap solution consisting of 10% glycerol in methanol with 0.01 mg/mL butylated hydroxytoluene. The samples were dried for 45 min in a speed vacuum at 35°C, the walls of the tubes were washed with 1 mL of hexane and re-dried until a small aqueous residue remained. The residue was dissolved in 80 μL of 80:20 water:acetonitrile with 0.1 mg/mL butylated hydroxytoluene and spin filtered with a 0.22-μm Millipore ultra-free filter. Samples were transferred to vials and 30 μL of sample was analyzed by liquid chromatography-tandem mass spectroscopy (LC-MS/MS) as described below. Sample extraction buffer was spiked and prepared identically to the samples with concentration ranges from 10 to 2500 pg/mL for PGE2 and 20-HETE.

Liquid Chromatography Followed by Tandem Mass Spectroscopy

Extracts were analyzed using a 5500 Q-TRAP hybrid/triple quadrupole linear ion trap mass spectrometer (SCIEX, Carlsbad, CA, United States) with electrospray ionization (ESI) in negative mode. The mass spectrometer was interfaced to a Shimadzu (Columbia, MD, United States) SIL-20AC XR auto-sampler followed by two LC-20AD XR LC pumps. The scheduled MRM transitions were monitored with a 1.5 min window. Optimal instrument parameters were determined by direct infusion of each analyte and are presented in the table below.

Analyte	Q1	Q3	RT	DP	EP	CE	CXP
PGE2	351.0	189.1	5.9	−85	−10	−26	−5
PGE2-d_9	360.2	280.2	5.9	−75	−10	−28	−11
20-HETE	319.1	289	10.3	−130	−10	−26	−11
20-HETE-d_6	325	281	10.3	−75	−10	−24	−9

Q1, Quadrupole Mass filter 1; Q3, Quadrupole Mass filter 3; RT, retention time; DP, declustering potential; EP, entrance potential; CE, collision energy; CXP, collision cell exit potential; PGE2-d_9 and 20-HETE-d_6, deuterium substituted versions of each compound used as internal standards.

The gradient mobile phase was delivered at a flow rate of 0.5 mL/min and consisted of two solvents, 0.05% acetic acid in water and acetonitrile. The analytes were resolved on a BetaBasic-C18 (100 × 2 mm, 3 μm) column at 40°C using the Shimadzu column oven. Data was acquired using Analyst 1.5.1 and analyzed using MultiQuant 3.0.1 (AB Sciex, ON, Canada). The lower limit of quantification was 10 pg/mL for both PGE2 and 20-HETE. As samples were blinded before sending them to the core laboratory, all measurements and analyses were performed blindly by default.

Protein Quantification

Protein quantification was performed using the Qubit 3.0 Fluorometer (Invitrogen/Thermo Fisher Scientific) on the 0.1 mL of homogenate prepared in 0.1% formic acid, as described in section "Preparation of Samples for 20-Hydroxyeicosatetraenoic Acid and Prostaglandin E2 Measurement." All reagents and materials were brought to room temperature before mixing to ensure optimal fluorescence and measurement accuracy. Qubit working solution and Qubit Standards 1, 2, and 3 were made fresh and calibration was performed using the fresh standards. Qubit working solution was prepared by diluting Qubit Protein Reagent 1:200 in Qubit Protein Buffer in a 15 mL Eppendorf. For each of the three standards and all samples, 190 μL of working solution and 10 μL of each standard were mixed by vortexing for 2–3 s. All samples rested at room temperature for 15 min following preparation. All readings were performed using the "Protein" function of the Qubit 3.0 fluorometer. Standard calibration was performed by measuring Standard 1, Standard 2, and Standard 3, in order. Only calibrations that produced a linear fluorescence curve were used for sample reading. The samples were split into multiple batches of 35 samples each, which allowed for the most accurate sample readings compared to the standards calibration. Immediately after calibration, each sample was read in order. Following completion of all samples in a single batch, samples were re-run from the beginning to determine the consistency of readings. The first and second readings were in close agreement. The average of both readings was used for all final comparisons.

Statistical Analyses

In all figures, data are shown as mean ± SEM with the raw data values indicated by individual points and the N indicated in parentheses. In our experience, the variability of responses observed at different regions (presumed regions of active pericyte control) along the same capillary is equal to that between different capillaries, slices, or animals. Therefore, capillary regions that constricted to 200 nM U46619 were used as the observational units in all slice experiments. Sample sizes were calculated based on previous experience with the experimental techniques used and expected variability. N indicates the number of pericyte regions studies in **Figures 1–4** and **Supplementary Figure 1**, the number of animals in **Figures 5C,D**, and the number of samples in **Figures 5E,F**. Normality of data was checked using the Kolmogorov–Smirnov test or D'Agostino-Pearson test and the equality of variance using the F-statistic. All normal data were compared using an analysis of variance (ANOVA) followed by Tukey's honest significant difference (HSD) test. Data in **Figure 5F** were non-normal, and therefore a Kruskal–Wallis test was used followed by Mann–Whitney test and Holm–Bonferroni multiple comparisons correction. Two-way ANOVA was used in

Figure 5C to test whether a significant interaction between stroke exposure and hemispheric CBF could be detected.
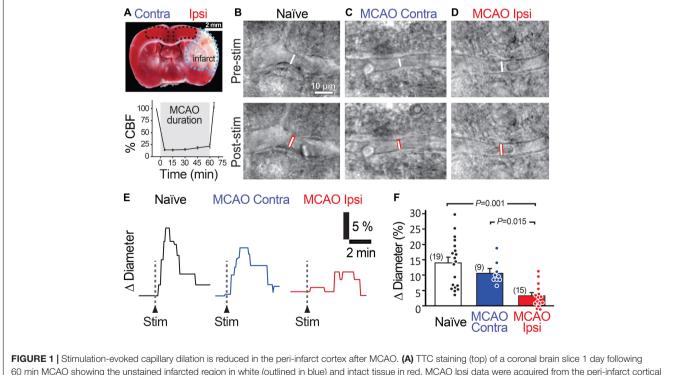
RESULTS

To assess neurovascular coupling in acute brain slices, we monitored changes in capillary diameter evoked by electrical stimulation of cortical neuronal activity (Mishra et al., 2016). We first confirmed that neuronal activity-evoked capillary dilation in adult (2-month-old) rat cortical slices by applying two different stimulation paradigms. We found that both high-frequency (100 Hz, 1 s) stimulation and low-frequency (20 Hz, 3 s) stimulation evoked robust capillary dilation (18.9 ± 4.7%, $n = 7$ from three animals, and 14.5 ± 1.8%, $n = 18$ from six animals, for high and low-frequency stimulation, respectively; **Supplementary Figure 1**). We previously showed that activity-dependent capillary dilation is mediated by an astrocytic signaling pathway dependent on the P2X1 receptor (Mishra et al., 2016). In our current experiments, bath application of the P2X1 inhibitor NF449 (100 nM) similarly reduced capillary dilation evoked by both high (3.9 ± 2.2%, $n = 6$ from two animals, $P = 0.01$) and low-frequency (1.9 ± 1.3%, $n = 20$ from four animals, $P = 0.00002$) stimulation (**Supplementary Figures 1B,D**). The low-frequency stimulation was chosen as a physiologically
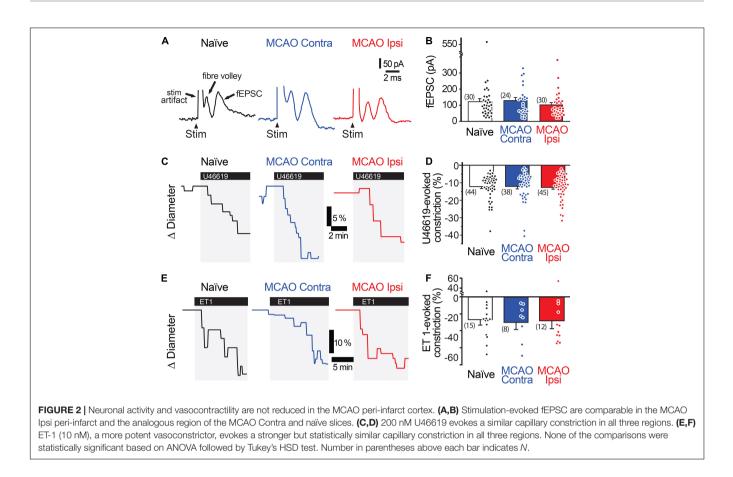
relevant minimal stimulation paradigm for all subsequent experiments (Tateno et al., 2004).

We next examined capillary responses evoked by low-frequency stimulation in the peri-infarct cortex of animals exposed to MCAO (MCAO Ipsi) and compared them to the analogous cortical region in contralateral slices (MCAO Contra) and slices from naïve animals (**Figure 1**). The baseline diameter of the capillaries across the three conditions was comparable (**Supplementary Table 1**). Stimulation evoked a capillary dilation of 14.0 ± 1.8% ($n = 19$ from six animals) in naïve cortex and 10.7 ± 1.3% ($n = 9$ from three animals, *n.s.* compared to naïve) in the MCAO Contra region, but this response was reduced to 3.3 ± 1.0% ($n = 15$ from four animals) in the MCAO Ipsi region (ANOVA $P = 0.00003$; Tukey's HSD $P = 0.001$ compared to naïve, $P = 0.015$ compared to MCAO Contra; **Figures 1E,F**).

Stimulation-evoked capillary responses may be reduced in the peri-infarct cortex for several reasons. The most parsimonious explanation is that neuronal activity is itself reduced. We tested this possibility by comparing the amplitude and rising slope of the stimulation-evoked fEPSCs (**Figures 2A,B**). The amplitude of the fEPSCs was 120.6 ± 19.6 nA ($n = 30$ from 14 animals) in naïve brains, 127.8 ± 18.8 nA ($n = 24$ from 10 animals) in the MCAO Contra region, and 100.8 ± 14.5 nA ($n = 30$ from 12 animals) in the MCAO Ipsi peri-infarct region (ANOVA $P = 0.6$). The rising slope of the fEPSCs was 80.7 ± 18.4 nA/ms in naïve brains, 101.5 ± 17.7 nA/ms in the MCAO Contra region,

FIGURE 1 | Stimulation-evoked capillary dilation is reduced in the peri-infarct cortex after MCAO. **(A)** TTC staining (top) of a coronal brain slice 1 day following 60 min MCAO showing the unstained infarcted region in white (outlined in blue) and intact tissue in red. MCAO Ipsi data were acquired from the peri-infarct cortical region and contralateral hemisphere and naïve brain slice data were acquired in the analogous region (outlined in black). Bottom graph shows the decrease in cerebral blood flow (CBF) in the MCA territory during occlusion. An example capillary in naïve **(B)**, MCAO Contra **(C)**, and MCAO Ipsi **(D)** cortex before (top) and after (bottom) neuronal stimulation. Dotted white lines show capillary diameter in U46619 prior to stimulation, while the underlaid red bars in lower panels show capillary diameter after stimulation. Example traces **(E)** and summary quantification **(F)** demonstrating the reduction in stimulation-evoked capillary dilation in the MCAO Ipsi peri-infarct cortex. *P*-values were obtained from ANOVA followed by Tukey's HSD test. Number in parentheses above each bar indicates *N*.
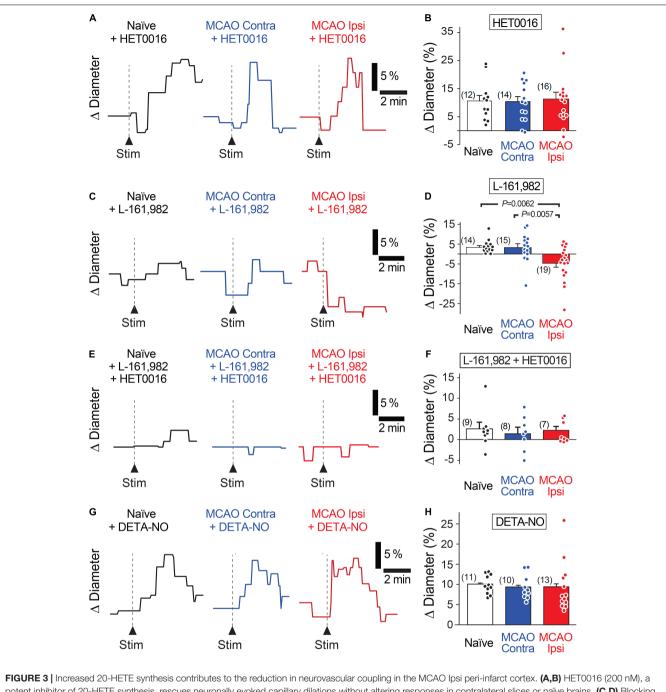
FIGURE 2 | Neuronal activity and vasocontractility are not reduced in the MCAO peri-infarct cortex. **(A,B)** Stimulation-evoked fEPSC are comparable in the MCAO Ipsi peri-infarct and the analogous region of the MCAO Contra and naïve slices. **(C,D)** 200 nM U46619 evokes a similar capillary constriction in all three regions. **(E,F)** ET-1 (10 nM), a more potent vasoconstrictor, evokes a stronger but statistically similar capillary constriction in all three regions. None of the comparisons were statistically significant based on ANOVA followed by Tukey's HSD test. Number in parentheses above each bar indicates N.

and 81.0 ± 11.2 nA/ms in the MCAO Ipsi peri-infarct region (ANOVA $P = 0.5$). A lack of vessel response could also be due to loss of vascular contractility. As dilation is in essence an inhibition of contraction, which is the active component of vascular regulation, we assessed vascular contractility by evaluating capillary constriction evoked by the thromboxane analog U46619 (**Figures 2C,D**). We found no difference between groups: U46619 (200 nM) evoked a constriction of $12.1 \pm 1.1\%$ ($n = 45$ from 13 animals) in naïve brains, $12.1 \pm 1.4\%$ ($n = 38$ from 11 animals) in the MCAO Contra region, and $12.6 \pm 1.1\%$ ($n = 45$ from 14 animals) in the MCAO Ipsi peri-infarct region (ANOVA $P = 0.9$). We further tested a second, stronger vasoconstrictor, endothelin 1 (ET-1, 10 nM), which also had a comparable effect across conditions (**Figures 2E,F**). ET-1 constricted capillaries by $26.7 \pm 6.4\%$ ($n = 15$ from four animals) in naïve brains, $30.1 \pm 8.5\%$ ($n = 8$ from three animals) in the MCAO Contra region, and $28.2 \pm 9.4\%$ ($n = 12$ from three animals) in the MCAO Ipsi region (ANOVA $P = 0.7$). Thus, the reduction in capillary dilation in the MCAO Ipsi peri-infarct cortex was not explained by a reduction in stimulation-evoked neuronal activity or loss of vasocontractility.

Increased levels of the vasoconstrictor 20-HETE in the plasma and cerebrospinal fluid correlate with worse prognosis in stroke patients (Crago et al., 2011; Yi et al., 2016, 2017). Thus, we tested whether 20-HETE underlies the reduction in evoked capillary dilation after MCAO by incubating acute brain slices in N-Hydroxy-N′-(4-butyl-2-methylphenyl) formamidine
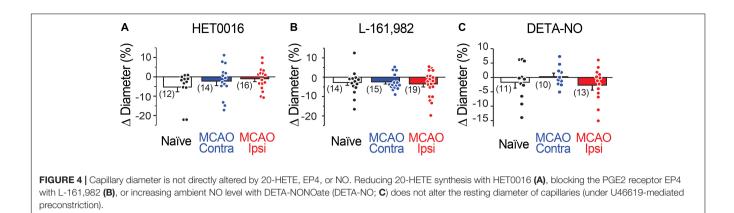
(HET0016, 200 nM) to inhibit 20-HETE synthesis prior to assaying neurovascular coupling (Miyata et al., 2001). Pre-incubation of slices with HET0016 completely rescued capillary neurovascular coupling in the MCAO peri-infarct region (**Figures 3A,B**). Stimulation-evoked capillary dilation in the presence of HET0016 was $10.4 \pm 2.0\%$ ($n = 12$ from three animals) in naïve brain slices, $10.1 \pm 1.8\%$ ($n = 14$ from four animals) in the MCAO Contra region, and $11.1 \pm 2.4\%$ ($n = 16$ from five animals) in the MCAO Ipsi peri-infarct region (ANOVA $P = 0.9$). HET0016 treatment did not directly alter the diameter of the vessels (**Figure 4A**).

As inhibition of 20-HETE synthesis revealed the presence of stimulation-evoked capillary dilation in the MCAO Ipsi peri-infarct cortex, we next sought to identify this dilatory signal. In healthy cortical tissue, capillary neurovascular coupling depends on PGE2 acting on its receptor EP4 (Hall et al., 2014; Mishra et al., 2016). If PGE2-dependent vasodilatory signaling persists after MCAO but is masked by coincidental synthesis of 20-HETE, then inhibiting the PGE2 pathway should reveal a stimulation-evoked constriction in the MCAO Ipsi peri-infarct cortex due to 20-HETE. Application of the EP4 receptor blocker L-161,982 (1 μM) to acute slices reduced neuronal stimulation-evoked capillary dilation in naïve brain slices ($3.3 \pm 0.9\%$; $n = 14$ from three animals) and in the MCAO Contra region ($3.2 \pm 1.8\%$; $n = 15$ from four animals; **Figures 3C,D**). In the MCAO Ipsi region, L-161,982 treatment converted stimulation-evoked capillary responses to

FIGURE 3 | Increased 20-HETE synthesis contributes to the reduction in neurovascular coupling in the MCAO Ipsi peri-infarct cortex. **(A,B)** HET0016 (200 nM), a potent inhibitor of 20-HETE synthesis, rescues neuronally evoked capillary dilations without altering responses in contralateral slices or naïve brains. **(C,D)** Blocking the EP4 receptor of PGE2 with L-161,982 (1 μM) unmasks a 20-HETE-mediated constriction only in the MCAO ipsilateral peri-infarct region. **(E,F)** Inhibiting EP4 receptors and 20-HETE synthesis simultaneously prevents capillary response to neuronal activation in all three conditions. **(G,H)** Increasing NO concentration in the tissue with DETA-NONOate (DETA-NO, 100 μM) restores stimulation-evoked capillary dilation in the MCAO ipsilateral hemisphere without altering capillary responses in contralateral or naïve brain slices. *P*-values were obtained from ANOVA followed by Tukey's HSD test. Number in parentheses above each bar indicates *N*.

constrictions as predicted ($-4.6 \pm 1.9\%$; $n = 19$ from six animals; ANOVA $P = 0.002$; Tukey's HSD $P = 0.006$ compared to naïve, $P = 0.005$ compared to MCAO Contra). L-161,982 did not affect baseline diameter (**Figure 4B**). When both 20-HETE and PGE2 pathways were simultaneously inhibited (200 nM HET0016 plus 1 μM L-161,982), stimulation-evoked responses

of either polarity were absent in all conditions (**Figures 3E,F**). The evoked change in capillary diameter measured $2.6 \pm 1.5\%$ ($n = 9$ from two animals) in naïve slices, $1.4 \pm 1.5\%$ ($n = 8$ from two animals) in the MCAO Contra region, and $2.1 \pm 0.9\%$ ($n = 8$ from two animals) in the MCAO Ipsi region (ANOVA $P = 0.8$).

FIGURE 4 | Capillary diameter is not directly altered by 20-HETE, EP4, or NO. Reducing 20-HETE synthesis with HET0016 **(A)**, blocking the PGE2 receptor EP4 with L-161,982 **(B)**, or increasing ambient NO level with DETA-NONOate (DETA-NO; **C**) does not alter the resting diameter of capillaries (under U46619-mediated preconstriction).

In healthy brains, CYP450 enzymes are inhibited by NO, which results in low levels of tissue 20-HETE (Hall et al., 2014). A reduction in neuronal and endothelial isoforms of NO synthase, leading to a decrease in activity-dependent NO production, is reported after ischemic injury (Zhao et al., 2018), which could lead to increased CYP450 activity. We reasoned that if disinhibition of CYP450s due to a decrease in NO is responsible for enhancing 20-HETE synthesis after MCAO, we should be able to rescue neurovascular coupling simply by exogenously raising NO concentration. To this end, we performed experiments in the presence of DETA-NONOate (100 µM), a long half-life NO donor that releases a reasonably constant amount of NO over several hours (Keefer et al., 1996). When NO levels were thus raised in slices, capillary neurovascular coupling was rescued (**Figures 3G,H**) comparably to when 20-HETE synthesis was inhibited, while having no direct effect on baseline capillary diameter (**Figure 4C**). Stimulation-evoked capillary dilation in the presence of DETA-NONOate was $10.1 \pm 0.7\%$ ($n = 11$ from three animals) in naïve slices, $9.4 \pm 0.9\%$ ($n = 10$ from six animals) in the MCAO Contra region, and $9.4 \pm 1.7\%$ ($n = 13$ from five animals) in the MCAO Ipsi peri-infarct region (ANOVA $P = 0.9$). The raw diameters of all capillaries used in HET0016, L-161,982, and DETA-NONOate experiments are reported in **Supplementary Table 1**.

We next sought to examine whether 20-HETE contributes to changes in CBF after stroke *in vivo*. We used ASL-MRI to map cortical perfusion in anesthetized rats before and 30 min after intravenous (i.v.) injection of HET0016 (1 mg/kg) or vehicle. The maps were corrected to largely reflect capillary blood flow (see section "Materials and Methods") and CBF was quantified in the MCAO Ipsi peri-infarct cortex and analogous regions of the MCAO Contra and naïve cortices (outlined in **Figures 5A,B**). CBF was significantly higher in the cortex of naïve rats compared to those exposed to MCAO in both hemispheres (**Figure 5C**; naïve: 36.4 ± 1.8 mL/100 g/min in Ipsi and 34.1 ± 2.0 mL/100 g/min in Contra, $n = 11$ animals; MCAO: 27.2 ± 2.5 mL/100 g/min in Ipsi and 27.3 ± 1.8 mL/100 g/min in Contra, $n = 10$ animals; two-way ANOVA $P = 0.0004$).
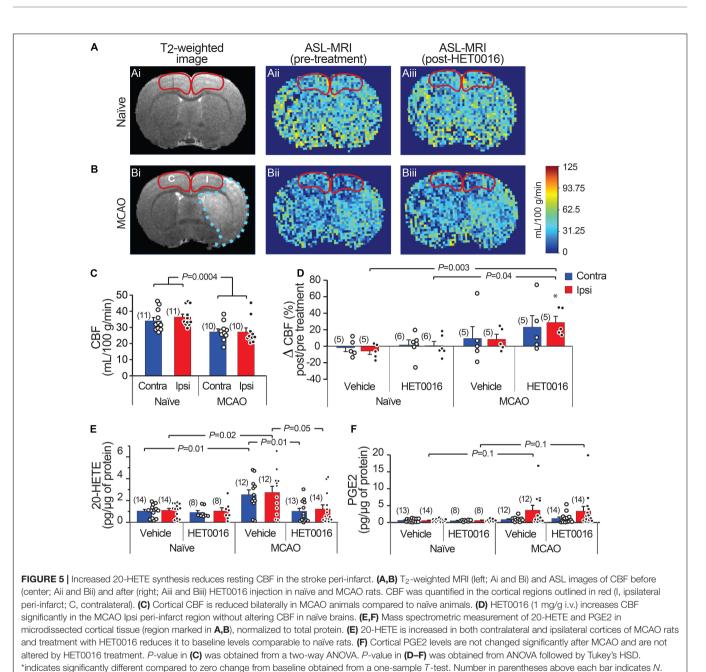
Acute delivery of HET0016 (i.v.) increased CBF in the MCAO brains bilaterally ($28.8 \pm 7.4\%$ increase in Ipsi and $23.2 \pm 14.1\%$ increase in Contra), but this change reached significance only in the MCAO Ipsi peri-infarct cortex (one-sample t-test $P = 0.009$

compared to zero change). The effect of HET0016 treatment on CBF in MCAO Ipsi cortex was in stark contrast to that observed in naïve cortices, where CBF changes were essentially absent (**Figure 5D**; ANOVA $P = 0.0036$). These data strongly support the idea that 20-HETE contributes to a decrease in cortical blood flow following MCAO, especially in the peri-infarct region. Vehicle treatment did not alter CBF in either hemisphere in naïve or MCAO rats. The changes in CBF observed after vehicle and HET0016 treatment for all regions are reported in **Table 1**.

Lastly, we harvested brains from vehicle- and HET0016-treated animals immediately after MRI to measure the levels of cortical 20-HETE and PGE2 in the same regions where CBF was quantified, reflecting the MCAO Ipsi peri-infarct region and analogous control cortices (outlined in **Figures 5A,B**). These regions were microdissected from coronal brain slices and processed for liquid chromatography followed by tandem mass spectrometry. The values obtained for each metabolite were normalized to total protein content in each sample and are reported in **Table 1**. 20-HETE was elevated by ~2.5-fold bilaterally in the cortex of vehicle-treated MCAO rats and acute treatment with HET0016 reduced 20-HETE to baseline levels (**Figure 5E**; ANOVA $P = 0.009$ for Ipsi, $P = 0.004$ for Contra). Interestingly, PGE2 levels were also increased, particularly in some samples, from the MCAO Ipsi region (non-parametric Kruskal–Wallis test, $P = 0.025$), though pairwise comparison of the data did not reveal a statistical significance between any groups (**Figure 5F**). Furthermore, cortical PGE2 levels were not altered by HET0016 treatment.

DISCUSSION

Our experiments show that capillary neurovascular coupling is reduced in cortical regions beyond the infarct after MCAO and that this reduction is due to increased synthesis of 20-HETE, a potent vasoconstrictor. PGE2-mediated dilation of capillaries was intact after transient MCAO and inhibition of 20-HETE synthesis with HET0016 allowed healthy activity-coupled PGE2-mediated capillary dilations to occur. Increasing NO, an inhibitor of 20-HETE synthesis, can similarly rescue capillary dilation. *In vivo*, 20-HETE levels were increased by 2.5-fold in the peri-infarct cortex of MCAO brains and correlated

FIGURE 5 | Increased 20-HETE synthesis reduces resting CBF in the stroke peri-infarct. **(A,B)** T_2-weighted MRI (left; Ai and Bi) and ASL images of CBF before (center; Aii and Bii) and after (right; Aiii and Biii) HET0016 injection in naïve and MCAO rats. CBF was quantified in the cortical regions outlined in red (I, ipsilateral peri-infarct; C, contralateral). **(C)** Cortical CBF is reduced bilaterally in MCAO animals compared to naïve animals. **(D)** HET0016 (1 mg/g i.v.) increases CBF significantly in the MCAO Ipsi peri-infarct region without altering CBF in naïve brains. **(E,F)** Mass spectrometric measurement of 20-HETE and PGE2 in microdissected cortical tissue (region marked in **A,B**), normalized to total protein. **(E)** 20-HETE is increased in both contralateral and ipsilateral cortices of MCAO rats and treatment with HET0016 reduces it to baseline levels comparable to naïve rats. **(F)** Cortical PGE2 levels are not changed significantly after MCAO and are not altered by HET0016 treatment. P-value in **(C)** was obtained from a two-way ANOVA. P-value in **(D–F)** was obtained from ANOVA followed by Tukey's HSD. *indicates significantly different compared to zero change from baseline obtained from a one-sample T-test. Number in parentheses above each bar indicates N.

with a decrease in cortical CBF. Inhibiting 20-HETE synthesis normalized 20-HETE levels and significantly increased CBF in the peri-infarct cortex. Our findings suggest that engagement of a 20-HETE-dependent vasoconstrictor pathway causes the loss of capillary neurovascular coupling, at least in part, in otherwise healthy peri-infarct cortical tissue following ischemic stroke (**Figure 6**).

Several clinical studies have demonstrated that stroke results not only in an acute loss of blood flow, and consequently tissue, within the infarcted region but also causes widespread dysfunction of neurovascular physiology beyond the lesion (Krainik et al., 2005; Lin et al., 2011; Salinet et al., 2015, 2018). Cerebral autoregulation, vascular reactivity, and neurovascular

coupling are significantly impaired even in regions far from the infarct. Our observations suggest that an increase in 20-HETE synthesis may contribute to the observed impairment in neurovascular coupling (**Figure 3**). Previous reports showing an increase in 20-HETE in the plasma of stroke patients and in the cerebrospinal fluid of subarachnoid hemorrhage patients who develop delayed cerebral ischemia support this notion (Crago et al., 2011; Yi et al., 2016, 2017). Pretreatment with 20-HETE inhibitors has been shown to attenuate the acute decrease in CBF (up to 240 min) following MCAO (Poloyac et al., 2006; Renic et al., 2009). Our studies imply that 20-HETE-mediated suppression of capillary neurovascular coupling is likely contributing to this decrease in CBF and

TABLE 1 | Changes in CBF and levels of cortical 20-HETE and PGE2 after vehicle or HET0016 treatment.

		Naïve Vehicle ($n = 5$ animals)	Naïve HET0016 ($n = 6$ animals)	MCAO Vehicle ($n = 5$ animals)	MCAO HET0016 ($n = 5$ animals)	ANOVA (P-value)
ΔCBF%	Ipsilateral	-5.9 ± 3.9	0.7 ± 5.1	8.4 ± 6.1	$28.8 \pm 7.4^{*\dagger\ddagger}$	**0.0036**
	Contralateral	-1.9 ± 4.6	1.6 ± 6.1	9.5 ± 14.3	23.2 ± 14.1	0.3678
20-HETE (pg/μg)	Ipsilateral	1.11 ± 0.17	1.04 ± 0.28	$2.74 \pm 0.57^{\dagger}$	$1.4 \pm 0.38^{\S}$	**0.0090**
	Contralateral	1.04 ± 0.15	0.91 ± 0.17	$2.54 \pm 0.43^{\dagger}$	$1.02 \pm 0.27^{\S}$	**0.0040**
PGE2 (pg/μg)	Ipsilateral	0.57 ± 0.11	0.58 ± 0.14	3.66 ± 1.43	3.36 ± 1.38	**0.0251**§§
	Contralateral	0.64 ± 0.13	0.52 ± 0.09	0.88 ± 0.19	1.19 ± 0.41	0.7824§§

*The changes in cortical CBF measured from ASL-MRI after vehicle or HET0016 treatment are reported as percent change from pre-treatment baseline (ΔCBF%). The levels of cortical 20-HETE and PGE2 measured by LC-MS/MS after vehicle or HET0016 treatment are reported as pg/μg total protein (tissue taken from the same animals in which ASL-MRI was performed, immediately following MRI). All measurements were made from the cortical region demarcated as peri-infarct (MCAO ipsilateral hemisphere) or analogous region (contralateral hemisphere and naïve brains), as shown in **Figures 1A, 5A,B**.*
$^{*}P < 0.01$, one sample t-test as compared to no change from baseline.
$^{\dagger}P < 0.05$, post hoc Tukey's HSD compared to Naïve vehicle.
$^{\ddagger}P < 0.05$, post hoc Tukey's HSD compared to Naïve HET0016.
$^{\S}P < 0.05$, post hoc Tukey's HSD compared to MCAO vehicle.
§§Kruskal–Wallis non-parametric ANOVA.
ANOVA P-values that were significant are indicated in bold.

that 20-HETE's effects on neurovascular coupling and CBF continue at least up to a day after stroke. Whether 20-HETE also contributes to deficits in autoregulation and vascular reactivity, and how long these effects last in the post-stroke brain, remain unknown. Importantly, however, the continued presence of a dilatory signaling pathway *via* EP4 suggests that inhibiting 20-HETE-dependent constriction may help restore peri-infarct neurovascular coupling without tonic effects on capillaries, which may prove a powerful and therapeutically relevant tool for future drug development efforts.

Emerging evidence highlights the crucial and multifaceted roles of pericytes in healthy brain function, including contributions to angiogenesis, immune function, blood-brain barrier integrity, and CBF regulation (reviewed in Sweeney et al., 2016; Eltanahy et al., 2021). Pericytes also allow neurovascular coupling to occur at the capillary level (Hall et al., 2014; Mishra et al., 2016). Experimentally, loss of pericytes can result in aberrant CBF, blood-brain barrier leakage, loss of neurovascular coupling (Kisler et al., 2017, 2020; Watson et al., 2020), and may lead to neurodegenerative phenotypes resembling AD (Sagare et al., 2013). Previous studies have shown that pericytes contract and even die in response to ischemia, potentially restricting reperfusion and preventing recovery (Yemisci et al., 2009; Hall et al., 2014). Our present findings provide additional support for pericytes as key regulators of capillary blood flow and suggest that functional dysregulation of pericytes due to increased 20-HETE signaling-mediated inhibition of activity-coupled relaxations may further contribute to the long-term effects of ischemic stroke even outside the infarct.

The absolute values of CBF measurements obtained from ASL-MRI depend on the specific ASL approach and radiofrequency coil technology used and therefore vary between studies conducted in humans and rodents. The FAIR ASL approach uses a global inversion pulse to label incoming blood with an efficiency that depends on the radiofrequency transmitter coil coverage caudal to the brain (Lipton et al., 2001). The transmitter coil length used in this study (6 cm)
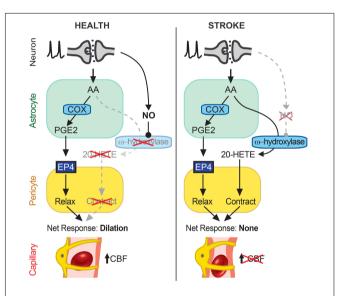

FIGURE 6 | Schematic summary of findings. In healthy cortical tissue (left), neuronal activity stimulates AA synthesis and downstream metabolism to PGE2 in astrocytes. PGE2 acts on EP4 receptors on pericytes to relax them and induce capillary dilation, thus allowing an activity-coupled increase in CBF to occur. 20-HETE synthesis is inhibited by NO, likely synthesized in an activity-dependent manner from neurons (26), which suppresses pericyte contraction. After stroke (right), AA in astrocytes continues to be metabolized to PGE2, which acts on EP4 receptors to relax pericytes, but the reduction in NO generation disinhibits a parallel AA metabolism pathway *via* CYP450 ω-hydroxylases to produce 20-HETE, which causes pericyte contraction. The cell type(s) in which CYP450 ω-hydroxylases are active remain unknown but may include both astrocytes and pericytes. The opposing effects of EP4-dependent relaxation and 20-HETE-induced contraction of pericytes result in no net change in capillary diameter and therefore no increase in CBF. Over time, this reduced neurovascular coupling could chronically impair resting CBF and contribute to cognitive decline.

generally results in near-complete inversion for mouse brains but only partial inversion for rat brains, thus producing lower CBF measurements in rats (Vallatos et al., 2018). The

absolute values of CBF obtained in our study fell within the range reported in other rat studies employing comparable radiofrequency coil technology (Drazanova et al., 2019). Changes in animal placement under the coil can also impact the values obtained; however, we took extreme care to center the head consistently within the volume transmitter coil to optimize inversion labeling and enable robust comparison between animals. Additionally, the strength of our analysis lies in the fact that the effects of HET0016 (and vehicle) were quantified as a change in CBF within the same region in each animal before and after treatment to preclude any confounds introduced by the imaging technology. Our perfusion quantification methods were further optimized to reflect microvascular flow, where we see a significant decrease after MCAO. This agrees with the reduced capillary perfusion observed even after recanalization in stroke patients (Al-Ali et al., 2016).

Several potential mechanisms could explain the observed increase in 20-HETE synthesis. The two foremost mechanisms are an increase in CYP450 ω-hydroxylase activity or upregulation of CYP450 ω-hydroxylase enzymes after stroke. In our *ex vivo* experiments, we observed that inhibiting 20-HETE synthesis had no effect on baseline capillary diameter (**Figure 4**), despite significantly enhancing stimulation-evoked dilation in the peri-infarct region (**Figures 3A,B**). This suggests that 20-HETE synthesis occurs in an activity-dependent manner. Furthermore, increasing NO levels to enhance inhibition of CYP450 ω-hydroxylases also rescued neurovascular coupling to its full extent (**Figures 3G,H**). These data support the former hypothesis – that the increase in 20-HETE synthesis is due to increased enzymatic activity – but do not entirely exclude the latter. Several CYP450 enzymes can ω-hydroxylate arachidonic acid to generate 20-HETE (Roman, 2002). Although the identity of these enzymes remains unknown, CYP4A and CYP4F have been implicated in 20-HETE synthesis in the brain (Roman, 2002). However, without selective reagents to study these enzymes (e.g., antibodies and inhibitors), determining the specific ω-hydroxylase(s) involved remains challenging. Future unbiased research using transcriptomic and proteomic analysis will be necessary to elucidate which ω-hydroxylase enzymes are expressed in the brain and possibly altered after stroke. Additionally, an oversupply of the substrate due to increased production of arachidonic acid could also increase 20-HETE production. Notably, human mutations in CYP450 hydroxylase enzymes, particularly CYP4A11 and CYP4F2, are linked with increased prevalence of ischemic stroke and hypertension (Fu et al., 2008; Deng et al., 2010; Fava et al., 2012; Roman and Fan, 2018), especially in males, while certain single nucleotide polymorphisms in CYP4F2 are associated with decreased 20-HETE production (Stec et al., 2007). These findings suggest that some individuals may be at higher risk for, or protected from, the negative impacts of ischemic stroke on neurovascular coupling. These polymorphisms in eicosanoid metabolizing CYP enzymes also appear to have sex-specific effects (Fava et al., 2012). Although our current study was not powered to test sex differences in the reduction in neurovascular coupling after stroke, this is certainly a question of interest for further study.

The cellular source of 20-HETE is also not entirely clear. Astrocytes are postulated to be the major source of arachidonic acid in the brain (Moore et al., 1991) and they express the necessary enzymes (Mishra et al., 2016). A recent study showed that the 20-HETE synthesizing enzyme CYP4A is expressed in astrocytes, vascular smooth muscle cells (VSMCs), pericytes, and endothelial cells, while the recently identified 20-HETE receptors GPR75 and GPR39 are both present on VSMCs and pericytes (Alkayed et al., 2018; Gonzalez-Fernandez et al., 2020). Being lipid-soluble, arachidonic acid could easily diffuse out of astrocytes and into other nearby cells for further metabolism. Expression of CYP4A isoforms increases in both astrocytes and VSMCs after ischemia (Dunn et al., 2008; Liu et al., 2019). Thus, 20-HETE synthesis in astrocytes, VSMCs, and pericytes may all potentially contribute to neurovascular coupling deficits. A recent human vascular transcriptome analysis showed that several other CYP450 enzymes capable of synthesizing 20-HETE are also present in cells within the neurovascular unit (Yang et al., 2021). In particular, CYP4Z1 is expressed in human pericytes while CYP4F3 and CYP4F11 are expressed in hippocampal and cortical astrocytes. Interestingly, CYP4Z1 (in pericytes) and CYP4F3 (in astrocytes) were both increased over twofold in AD patients (Yang et al., 2021). Whether this results in an increased 20-HETE burden and contributes to the vascular dysfunction observed in AD is an avenue for future research.

The fact that CYP4A expression increases in astrocytes and VSMCs after ischemia and that 20-HETE appears necessary for mounting an appropriate angiogenic response (Liu et al., 2019) suggests that 20-HETE may be beneficial in some contexts after stroke. However, prolonged overproduction of 20-HETE and its negative effects on neurovascular coupling could render this response detrimental. A better understanding of the balance between the beneficial and harmful effects of 20-HETE may help determine when and to what extent its synthesis should be inhibited post-stroke to maximize clinical outcomes.

Our findings show that neurovascular coupling is reduced only in the ipsilesional peri-infarct regions of rats exposed to MCAO, 1 day after the ischemic insult. Yet, we found that 20-HETE increases in both hemispheres (**Figure 5E**) and contributes to lower CBF bilaterally after MCAO (**Figures 5C,D**). 20-HETE has important roles in many other signaling processes, including a dual role in the initiation and resolution of inflammation (Johnson et al., 2015). The presence of 20-HETE in the contralateral hemisphere at the early time point studied herein may be related to an inflammatory response rather than vascular regulation. Further, we used whole tissue homogenates to measure 20-HETE levels with the assumption that tissue amounts should reflect the overall biological availability of an easily diffusible lipid signaling mediator. However, the cellular location of 20-HETE synthesis and action could determine which specific physiological processes it can alter. Notably, impairments in neurovascular coupling in stroke patients have also been reported either exclusively ipsilateral to the lesion (Krainik et al., 2005) or bilaterally, both in the lesioned and unlesioned hemispheres (Salinet et al., 2015, 2018). The reduction in neurovascular coupling may initially only occur in the stroke hemisphere but then spread to the contralateral hemisphere

at later time points. Our finding that 20-HETE is increased bilaterally may predict a worsening of neurovascular coupling over time, in particular spreading to the contralateral hemisphere, and future work is needed to test this suggestion. Changes in neurovascular coupling at this early period after stroke could also be occurring at the level of larger vessels, which were not tested in our study but may explain the difference between our *ex vivo* observations in neurovascular coupling (capillary focused) and our *in vivo* observations in global CBF (which was optimized to largely, but not exclusively, reflect capillary flow). Although our studies focused on 20-HETE-dependent suppression of neurovascular coupling, 20-HETE may not be the sole driver of this impairment; thus, other mechanisms should also be investigated in future studies.

CONCLUSION

In conclusion, our findings suggest that ischemic stroke suppresses activity-dependent capillary dilation in peri-infarct regions beyond the primary infarct, possibly providing a mechanistic basis for the long-lasting cerebrovascular deficits and neurological deterioration observed in stroke patients. This reduction in neurovascular coupling appears to be the result of an increase in 20-HETE synthesis by ω-hydroxylases, which masked an otherwise healthy vasoactive response governed by PGE2 signaling. The persistence of the dilatory signaling pathway further suggests that it may be possible to pharmacologically restore neurovascular coupling following stroke.

DATA AVAILABILITY STATEMENT

The raw data supporting the conclusions of this article will be made available by the authors, without undue reservation.

ETHICS STATEMENT

The animal study was reviewed and approved by the Oregon Health & Science University Institutional Animal Care and Use Committee.

AUTHOR CONTRIBUTIONS

ZL performed all *ex vivo* slice experiments. HM performed and analyzed all ASL-MRI *in vivo* experiments. MP supervised all MRI experiments and analyses. HM and TS prepared the tissue samples for LC-MS/MS and protein quantification. AM conceived of the project, assisted with experiments, analyzed the data, and drafted the manuscript. All authors contributed to editing the manuscript.

FUNDING

ACKNOWLEDGMENTS

SUPPLEMENTARY MATERIAL

The Supplementary Material for this article can be found online at: https://www.frontiersin.org/articles/10.3389/fncel.2021.762843/full#supplementary-material

REFERENCES

Al-Ali, F., Berkhemer, O. A., Yousman, W. P., Elias, J. J., Bender, E. N., Lingsma, H. F., et al. (2016). The capillary index score as a marker of viable cerebral tissue: proof of concept-the capillary index score in the MR CLEAN (Multicenter Randomized Clinical Trial of Endovascular Treatment for Acute Ischemic Stroke in the Netherlands) trial. *Stroke* 47, 2286–2291. doi: 10.1161/STROKEAHA.116.013513

Alkayed, N. J., Cao, Z., Qian, Z. Y., Nagarajan, S., Liu, X., Nelson, J., et al. (2018). Bidirectional control of coronary vascular resistance by eicosanoids via a novel GPCR. *bioRxiv* [preprint]. doi: 10.1101/420406

Alonso-Galicia, M., Drummond, H. A., Reddy, K. K., Falck, J. R., and Roman, R. J. (1997). Inhibition of 20-HETE production contributes to the vascular responses to nitric oxide. *Hypertension* 29, 320–325. doi: 10.1161/01.hyp.29.1.320

Attwell, D., Buchan, A. M., Charpak, S., Lauritzen, M., Macvicar, B. A., and Newman, E. A. (2010). Glial and neuronal control of brain blood flow. *Nature* 468, 232–243. doi: 10.1038/nature09613

Crago, E. A., Thampatty, B. P., Sherwood, P. R., Kuo, C. W., Bender, C., Balzer, J., et al. (2011). Cerebrospinal fluid 20-HETE is associated with delayed cerebral ischemia and poor outcomes after aneurysmal subarachnoid hemorrhage. *Stroke* 42, 1872–1877. doi: 10.1161/STROKEAHA.110.605816

Deng, S., Zhu, G., Liu, F., Zhang, H., Qin, X., Li, L., et al. (2010). CYP4F2 gene V433M polymorphism is associated with ischemic stroke in the male Northern Chinese Han population. *Prog. Neuropsychopharmacol. Biol. Psychiatry* 34, 664–668. doi: 10.1016/j.pnpbp.2010.03.009

Drazanova, E., Ruda-Kucerova, J., Kratka, L., Stark, T., Kuchar, M., Maryska, M., et al. (2019). Different effects of prenatal MAM vs. perinatal THC exposure on regional cerebral blood perfusion detected by Arterial Spin Labelling MRI in rats. *Sci. Rep.* 9:6062. doi: 10.1038/s41598-019-42532-z

Dunn, K. M., Renic, M., Flasch, A. K., Harder, D. R., Falck, J., and Roman, R. J. (2008). Elevated production of 20-HETE in the cerebral vasculature contributes to severity of ischemic stroke and oxidative stress in spontaneously hypertensive rats. *Am. J. Physiol. Heart Circ. Physiol.* 295, H2455–H2465. doi: 10.1152/ajpheart.00512.2008

Eltanahy, A. M., Koluib, Y. A., and Gonzales, A. (2021). Pericytes: intrinsic transportation engineers of the CNS microcirculation. *Front. Physiol.* 12:719701. doi: 10.3389/fphys.2021.719701

Fava, C., Ricci, M., Melander, O., and Minuz, P. (2012). Hypertension, cardiovascular risk and polymorphisms in genes controlling the cytochrome P450 pathway of arachidonic acid: a sex-specific relation? *Prostaglandins Other Lipid Mediat.* 98, 75–85. doi: 10.1016/j.prostaglandins.2011.11.007

Fordsmann, J. C., Ko, R. W., Choi, H. B., Thomsen, K., Witgen, B. M., Mathiesen, C., et al. (2013). Increased 20-HETE synthesis explains reduced cerebral blood flow but not impaired neurovascular coupling after cortical spreading depression in rat cerebral cortex. *J. Neurosci.* 33, 2562–2570. doi: 10.1523/JNEUROSCI.2308-12.2013

Fu, Z., Nakayama, T., Sato, N., Izumi, Y., Kasamaki, Y., Shindo, A., et al. (2008). Haplotype-based case study of human CYP4A11 gene and cerebral infarction in Japanese subject. *Endocrine* 33, 215–222. doi: 10.1007/s12020-008-9078-6

Gonzalez-Fernandez, E., Staursky, D., Lucas, K., Nguyen, B. V., Li, M., Liu, Y., et al. (2020). 20-HETE enzymes and receptors in the neurovascular unit: implications in cerebrovascular disease. *Front. Neurol.* 11:983. doi: 10.3389/fneur.2020.00983

Gordon, G. R., Choi, H. B., Rungta, R. L., Ellis-Davies, G. C., and Macvicar, B. A. (2008). Brain metabolism dictates the polarity of astrocyte control over arterioles. *Nature* 456, 745–749. doi: 10.1038/nature07525

Hall, C. N., Reynell, C., Gesslein, B., Hamilton, N. B., Mishra, A., Sutherland, B. A., et al. (2014). Capillary pericytes regulate cerebral blood flow in health and disease. *Nature* 508, 55–60. doi: 10.1038/nature13165

Iadecola, C. (2017). The neurovascular unit coming of age: a journey through neurovascular coupling in health and disease. *Neuron* 96, 17–42. doi: 10.1016/j.neuron.2017.07.030

Iturria-Medina, Y., Sotero, R. C., Toussaint, P. J., Mateos-Perez, J. M., Evans, A. C., and Alzheimer's Disease Neuroimaging Initiative (2016). Early role of vascular dysregulation on late-onset Alzheimer's disease based on multifactorial data-driven analysis. *Nat Commun* 7, 11934. doi: 10.1038/ncomms11934

Johnson, A. L., Edson, K. Z., Totah, R. A., and Rettie, A. E. (2015). Cytochrome P450 omega-hydroxylases in inflammation and cancer. *Adv. Pharmacol.* 74, 223–262. doi: 10.1016/bs.apha.2015.05.002

Joo, I. L., Lai, A. Y., Bazzigaluppi, P., Koletar, M. M., Dorr, A., Brown, M. E., et al. (2017). Early neurovascular dysfunction in a transgenic rat model of Alzheimer's disease. *Sci. Rep.* 7:46427. doi: 10.1038/srep46427

Keefer, L. K., Nims, R. W., Davies, K. M., and Wink, D. A. (1996). "NONOates" (1-substituted diazen-1-ium-1,2-diolates) as nitric oxide donors: convenient nitric oxide dosage forms. *Methods Enzymol.* 268, 281–293. doi: 10.1016/s0076-6879(96)68030-6

Kim, S. G. (1995). Quantification of relative cerebral blood flow change by flow-sensitive alternating inversion recovery (FAIR) technique: application to functional mapping. *Magn. Reson. Med.* 34, 293–301. doi: 10.1002/mrm.1910340303

Kisler, K., Nelson, A. R., Rege, S. V., Ramanathan, A., Wang, Y., Ahuja, A., et al. (2017). Pericyte degeneration leads to neurovascular uncoupling and limits oxygen supply to brain. *Nat. Neurosci.* 20, 406–416. doi: 10.1038/nn.4489

Kisler, K., Nikolakopoulou, A. M., Sweeney, M. D., Lazic, D., Zhao, Z., and Zlokovic, B. V. (2020). Acute ablation of cortical pericytes leads to rapid neurovascular uncoupling. *Front. Cell. Neurosci.* 14:27. doi: 10.3389/fncel.2020.00027

Korte, N., Nortley, R., and Attwell, D. (2020). Cerebral blood flow decrease as an early pathological mechanism in Alzheimer's disease. *Acta Neuropathol.* 140, 793–810. doi: 10.1007/s00401-020-02215-w

Kotliar, K., Hauser, C., Ortner, M., Muggenthaler, C., Diehl-Schmid, J., Angermann, S., et al. (2017). Altered neurovascular coupling as measured by optical imaging: a biomarker for Alzheimer's disease. *Sci. Rep.* 7:12906. doi: 10.1038/s41598-017-13349-5

Krainik, A., Hund-Georgiadis, M., Zysset, S., and von Cramon, D. Y. (2005). Regional impairment of cerebrovascular reactivity and BOLD signal in adults after stroke. *Stroke* 36, 1146–1152. doi: 10.1161/01.STR.0000166178.40973.a7

Levine, D. A., Galecki, A. T., Langa, K. M., Unverzagt, F. W., Kabeto, M. U., Giordani, B., et al. (2015). Trajectory of cognitive decline after incident stroke. *JAMA* 314, 41–51. doi: 10.1001/jama.2015.6968

Lin, W. H., Hao, Q., Rosengarten, B., Leung, W. H., and Wong, K. S. (2011). Impaired neurovascular coupling in ischaemic stroke patients with large or small vessel disease. *Eur. J. Neurol.* 18, 731–736. doi: 10.1111/j.1468-1331.2010.03262.x

Lipton, M. L., Branch, C. A., Hrabe, J., Lewis, D. P., and Helpern, J. A. (2001). RF excitation profiles with FAIR: impact of truncation of the arterial input function on quantitative perfusion. *J. Magn. Reson. Imaging* 13, 207–214. doi: 10.1002/1522-2586(200102)13:2<207::aid-jmri1031>3.0.co;2-0

Liu, Y., Li, Y., Zhan, M., Liu, Y., Li, Z., Li, J., et al. (2019). Astrocytic cytochrome P450 4A/20-hydroxyeicosatetraenoic acid contributes to angiogenesis in the experimental ischemic stroke. *Brain Res.* 1708, 160–170. doi: 10.1016/j.brainres.2018.12.023

Longa, E. Z., Weinstein, P. R., Carlson, S., and Cummins, R. (1989). Reversible middle cerebral artery occlusion without craniectomy in rats. *Stroke* 20, 84–91. doi: 10.1161/01.str.20.1.84

Miklossy, J. (2003). Cerebral hypoperfusion induces cortical watershed microinfarcts which may further aggravate cognitive decline in Alzheimer's disease. *Neurol. Res.* 25, 605–610. doi: 10.1179/016164103101202048

Mishra, A. (2017). Binaural blood flow control by astrocytes: listening to synapses and the vasculature. *J. Physiol.* 595, 1885–1902. doi: 10.1113/JP270979

Mishra, A., Hamid, A., and Newman, E. A. (2011). Oxygen modulation of neurovascular coupling in the retina. *Proc. Natl. Acad. Sci. U.S.A* 108, 17827–17831. doi: 10.1073/pnas.1110533108

Mishra, A., O'Farrell, F. M., Reynell, C., Hamilton, N. B., Hall, C. N., and Attwell, D. (2014). Imaging pericytes and capillary diameter in brain slices and isolated retinae. *Nat. Protoc.* 9, 323–336. doi: 10.1038/nprot.2014.019

Mishra, A., Reynolds, J. P., Chen, Y., Gourine, A. V., Rusakov, D. A., and Attwell, D. (2016). Astrocytes mediate neurovascular signaling to capillary pericytes but not to arterioles. *Nat. Neurosci.* 19, 1619–1627. doi: 10.1038/nn.4428

Miyata, N., Taniguchi, K., Seki, T., Ishimoto, T., Sato-Watanabe, M., Yasuda, Y., et al. (2001). HET0016, a potent and selective inhibitor of 20-HETE synthesizing enzyme. *Br. J. Pharmacol.* 133, 325–329. doi: 10.1038/sj.bjp.0704101

Moore, S. A., Yoder, E., Murphy, S., Dutton, G. R., and Spector, A. A. (1991). Astrocytes, not neurons, produce docosahexaenoic acid (22:6 omega-3) and arachidonic acid (20:4 omega-6). *J. Neurochem.* 56, 518–524. doi: 10.1111/j.1471-4159.1991.tb08180.x

Nelson, A. R., Sweeney, M. D., Sagare, A. P., and Zlokovic, B. V. (2016). Neurovascular dysfunction and neurodegeneration in dementia and Alzheimer's disease. *Biochim. Biophys. Acta* 1862, 887–900. doi: 10.1016/j.bbadis.2015.12.016

Poloyac, S. M., Zhang, Y., Bies, R. R., Kochanek, P. M., and Graham, S. H. (2006). Protective effect of the 20-HETE inhibitor HET0016 on brain damage after temporary focal ischemia. *J. Cereb. Blood Flow Metab.* 26, 1551–1561. doi: 10.1038/sj.jcbfm.9600309

Renic, M., Klaus, J. A., Omura, T., Kawashima, N., Onishi, M., Miyata, N., et al. (2009). Effect of 20-HETE inhibition on infarct volume and cerebral blood flow after transient middle cerebral artery occlusion. *J. Cereb. Blood Flow Metab.* 29, 629–639. doi: 10.1038/jcbfm.2008.156

Roman, R. J. (2002). P-450 metabolites of arachidonic acid in the control of cardiovascular function. *Physiol. Rev.* 82, 131–185. doi: 10.1152/physrev.00021.2001

Roman, R. J., and Fan, F. (2018). 20-HETE: hypertension and beyond. *Hypertension* 72, 12–18. doi: 10.1161/HYPERTENSIONAHA.118.10269

Sagare, A. P., Bell, R. D., Zhao, Z., Ma, Q., Winkler, E. A., Ramanathan, A., et al. (2013). Pericyte loss influences Alzheimer-like neurodegeneration in mice. *Nat. Commun.* 4:2932. doi: 10.1038/ncomms3932

Salinet, A. S., Robinson, T. G., and Panerai, R. B. (2015). Effects of cerebral ischemia on human neurovascular coupling, CO2 reactivity, and dynamic cerebral autoregulation. *J. Appl. Physiol. (1985)* 118, 170–177. doi: 10.1152/japplphysiol.00620.2014

Salinet, A. S., Silva, N. C., Caldas, J., de Azevedo, D. S., de-Lima-Oliveira, M., Nogueira, R. C., et al. (2018). Impaired cerebral autoregulation and neurovascular coupling in middle cerebral artery stroke: influence of severity?

J. Cereb. Blood Flow Metab. 39, 2277–2285. doi: 10.1177/0271678X187
94835

Savva, G. M., Stephan, B. C., and Alzheimer's Society Vascular Dementia Systematic
Review Group (2010). Epidemiological studies of the effect of stroke on incident
dementia: a systematic review. *Stroke* 41, e41–e46. doi: 10.1161/STROKEAHA.
109.559880

Snowdon, D. A., Greiner, L. H., Mortimer, J. A., Riley, K. P., Greiner, P. A.,
and Markesbery, W. R. (1997). Brain infarction and the clinical expression of
Alzheimer disease. The Nun Study. *JAMA* 277, 813–817.

Stec, D. E., Roman, R. J., Flasch, A., and Rieder, M. J. (2007). Functional
polymorphism in human CYP4F2 decreases 20-HETE production. *Physiol.
Genomics* 30, 74–81. doi: 10.1152/physiolgenomics.00003.2007

Sweeney, M. D., Ayyadurai, S., and Zlokovic, B. V. (2016). Pericytes of the
neurovascular unit: key functions and signaling pathways. *Nat. Neurosci.* 19,
771–783. doi: 10.1038/nn.4288

Tateno, T., Harsch, A., and Robinson, H. P. (2004). Threshold firing frequency-
current relationships of neurons in rat somatosensory cortex: type 1 and
type 2 dynamics. *J. Neurophysiol.* 92, 2283–2294. doi: 10.1152/jn.0010
9.2004

Vallatos, A., Gilmour, L., Chalmers, A. J., and Holmes, W. M. (2018).
Multiple boli arterial spin labeling for high signal-to-noise rodent brain
perfusion imaging. *Magn. Reson. Med.* 79, 1020–1030. doi: 10.1002/mrm.
26706

van Rooij, F. G., Kessels, R. P., Richard, E., De Leeuw, F. E., and van Dijk, E. J.
(2016). Cognitive impairment in transient ischemic attack patients: a systematic
review. *Cerebrovasc. Dis.* 42, 1–9. doi: 10.1159/000444282

Vermeer, S. E., Longstreth, W. T. Jr., and Koudstaal, P. J. (2007). Silent brain
infarcts: a systematic review. *Lancet Neurol.* 6, 611–619. doi: 10.1016/S1474-
4422(07)70170-9

Watson, A. N., Berthiaume, A. A., Faino, A. V., McDowell, K. P., Bhat,
N. R., Hartmann, D. A., et al. (2020). Mild pericyte deficiency is associated
with aberrant brain microvascular flow in aged PDGFRbeta(+/-) mice.
J. Cereb. Blood Flow Metab. 40, 2387–2400. doi: 10.1177/0271678X199
00543

Yang, A. C., Vest, R. T., Kern, F., Lee, D. P., Maat, C. A., Losada, P. M., et al. (2021).
A human brain vascular atlas reveals diverse cell mediators of Alzheimer's
disease risk. *bioRxiv* [preprint]. doi: 10.1101/2021.04.26.441262

Yang, J., Wong, A., Wang, Z., Liu, W., Au, L., Xiong, Y., et al. (2015). Risk factors
for incident dementia after stroke and transient ischemic attack. *Alzheimers
Dement.* 11, 16–23. doi: 10.1016/j.jalz.2014.01.003

Yemisci, M., Gursoy-Ozdemir, Y., Vural, A., Can, A., Topalkara, K., and Dalkara,
T. (2009). Pericyte contraction induced by oxidative-nitrative stress impairs
capillary reflow despite successful opening of an occluded cerebral artery. *Nat.
Med.* 15, 1031–1037. doi: 10.1038/nm.2022

Yi, X., Han, Z., Zhou, Q., Lin, J., and Liu, P. (2016). 20-hydroxyeicosatetraenoic
acid as a predictor of neurological deterioration in acute minor
ischemic stroke. *Stroke* 47, 3045–3047. doi: 10.1161/STROKEAHA.116.0
15146

Yi, X., Lin, J., Wang, C., and Zhou, Q. (2017). CYP genetic variants, CYP
metabolite levels, and neurologic deterioration in acute ischemic stroke in
Chinese population. *J. Stroke Cerebrovasc. Dis.* 26, 969–978. doi: 10.1016/j.
jstrokecerebrovasdis.2016.11.004

Zhao, X., Liu, J., Yang, S., Song, D., Wang, C., Chen, C., et al. (2018). A
novel pharmacodynamic model in rats for preventing vascular dementia from
maintaining neurovascular coupling sensitivity. *Eur. J. Pharmacol.* 827, 149–
158. doi: 10.1016/j.ejphar.2018.03.010